

# EVALUATION OF REFRIGERANT OIL SEPARATORS FOR SCREW CHILLER

by

*Amey S. MAJGAONKAR*<sup>1,2\*</sup>, *A. KARTHIKEYAN*<sup>1</sup>, *Virendra K. BHOJWANI*<sup>3</sup>

<sup>1</sup> *Sathyabama Institute of Science and Technology, Chennai, Tamilnadu 600119, India*

<sup>2</sup> *Kirloskar Chillers Pvt. Ltd., Rajewadi, Satara, Maharashtra, 412801 India*

<sup>3</sup> *MITADT University, Loni, Pune Maharashtra, 412201, India*

\* Corresponding author; E-mail: amey.majgaonkar@kirloskar.com

*Effective refrigerant and oil separation is must for reliable and energy efficient chiller operation. Type A is a conventional oil separator design having a larger shell diameter and single refrigerant outlet connected to condenser using a discharge piping. Type B is novel oil separator design having a smaller shell diameter and two refrigerant outlets connected to the condenser. Computational fluid dynamics simulation of both designs is done for comparing oil separation efficiencies, velocity distribution, pressure drop and oil droplet trajectories. The simulated pressure drop matches closely (< 5 %) with experimental results in both designs. Type A design has higher (10912 Pa) pressure drop than Type B design. Simulation shows both the designs have almost equivalent oil separation efficiency at and above 25  $\mu\text{m}$  oil droplet sizes. Below 25  $\mu\text{m}$  oil droplet sizes, the Type B design has better oil separation efficiency. Chiller with Type B design has better oil circulation rates in liquid refrigerant than the chiller with Type A design at maximum flow rate condition. Therefore, Type B oil separator is found to be superior in performance (lower pressure drop and lower oil circulation rates) at lesser cost. Chiller with Type B oil separator is having 0.5 % more refrigeration capacity, 1.6 % higher Coefficient of performance and 1.1 % lower power consumption than chiller with Type A oil separator.*

*Keywords: Computational Fluid Dynamics (CFD), Discrete Phase Modelling (DPM), Separation Efficiency, Oil circulation rate (OCR), Chiller*

## 1. Introduction

Even a marginal improvement in chiller's efficiency has significant impact on global energy consumption and environment. The work motivation is to develop more efficient chillers at lower cost. Screw chillers use oil for lubrication, sealing, absorbing compression heat, reducing pulsations & slide valve control. Unseparated oil from the discharge gas lowers chiller performance. The oil percentage in

the refrigerant & oil mixture flow rate is referred as oil circulation rate (OCR). Good oil separator keeps the OCR lower than 0.5% by weight. Fig. 1 shows the screw chillers with the two oil separator concepts.

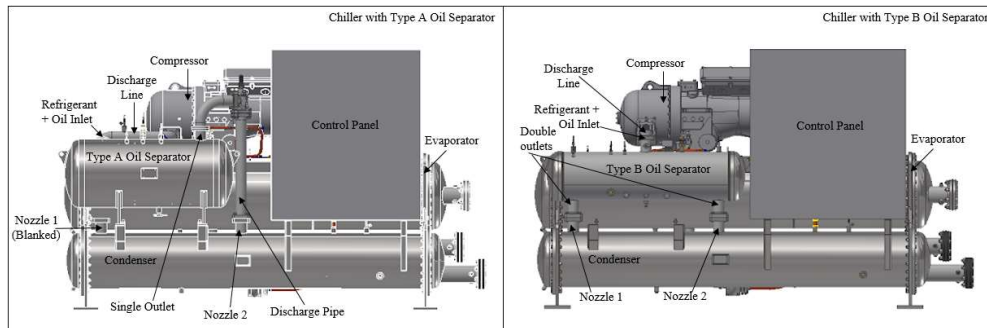


**Figure 1: Water-cooled screw chillers with Type A & Type B oil separators**

Oil separator needs to have lower pressure drop, better oil separation efficiency, smaller size and lesser cost. The objectives are relative evaluation of the Type A and Type B designs. Haider et al [1] proposed a OCR measurement method using an oil separator. They explained that separation efficiencies cannot be the only metrics for oil separator performance due to the refrigerant-oil solubility and miscibility. CFD analysis scope is limited to relatively comparison of oil separation efficiencies rather than finding their absolute performance. Oil circulation rate (OCR) in liquid refrigerant is experimentally determined and compared at maximum flow rate conditions for the two designs.

## 2. Computational Fluid Dynamics Modeling

### 2.1 Literature Review

Conventionally oil separators are sized as per API 12J [2], or Arnold and Stewart method [3]. Jekel et al [4] summarized & presented the gravity separation fundamentals. Bent Wiencke [5] proposed a theoretical model for computing separation velocities and separation distance for sizing the separators. Bothamley [6-7] presented performance quantification for gas-liquid separator components like feed pipe, inlet device, gas gravity separation section, demister & liquid gravity separator section.

Xu and Hrnjak [8] analyzed the formation, distribution, and movement of oil droplets inside the discharge plenum of a scroll compressor using Discrete Phase Model (DPM) with droplet size distribution captured by flow visualization. Xu and Hrnjak [9] found that the separation efficiency of coalescing type oil separator decreases with increase in vapor velocity along with rise in pressure drop.

Laleh et al [10] provided a detailed review on CFD studies of multiphase separators. Laleh et al [11] combined Volume of Fluid (VOF)- Discrete Phase Model (DPM) approach to capture both macroscopic and microscopic features of the phase-separation phenomenon. Gaffarkhah et al [12] did CFD analysis of three phase oil filled separator to compare separation performance and internal flow behavior using different semi-empirical methods. They used VOF and DPM models combined with  $k-\epsilon$  turbulence model to analyze separation performance. Oliveira Jr et al [13] performed numerical

simulations for demisters for application in gravity separators. They found velocity distribution and droplet mass on demister surface for various separator-demister configurations.

Feng et al [14] investigated the oil-gas separation in a horizontal separator using DPM approach for the simulation and laser diffraction technique to measure the oil concentration. The flow trajectories, separation efficiencies for different oil droplet diameters were analyzed. Wang et al [15] analyzed the internal flow fields in air-oil separator considering single phase flow. Eastwick et al [16] computationally analyzed aero engine air oil separator using DPM approach.

## 2.2 Geometry of oil separators with discharge piping

Fig. 2 shows simplified normalized geometry of oil separators with discharge piping. Discharge gas containing oil strikes the end casing wall of conventional Type A oil separator or shell of novel Type B oil separator. After an initial strike, its travel direction is reversed and velocity is significantly reduced as it travels through larger cross-sectional area, increasing the droplet's residence time to settle by gravity. Oil droplets adhere to the obstructing internal surface of shell and baffles. Gravity, flow obstructions and momentum change effectively separates the oil droplets reducing the load on demister. Demisters are effective above 10  $\mu\text{m}$  oil droplet sizes.

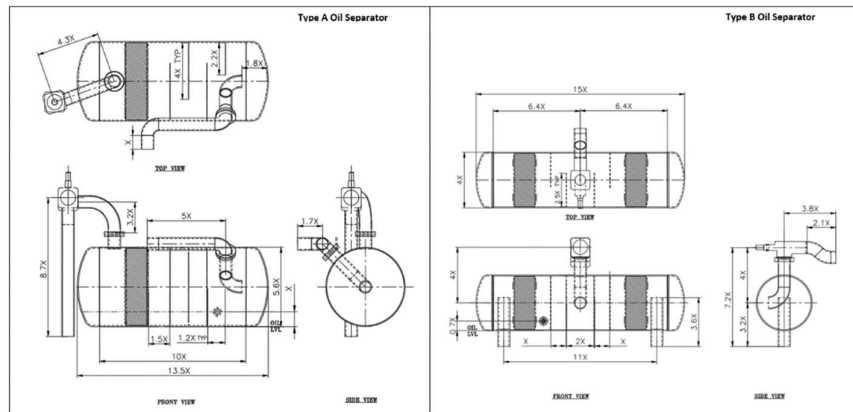


Figure 2: Geometry of oil separators with discharge piping

## 2.3 Inputs for CFD

The refrigerant and oil properties used in simulation are given in tab. 1.

Table 1: Refrigerant and oil properties

Parameter	Unit	R134a	Oil
Pressure	bar abs	9.12	9.12
Temperature	$^{\circ}\text{C}$	49.73	49.73
Flow rate	$\text{m}^3\text{s}^{-1}$	0.0765	$2.343 \times 10^{-3}$
Density	$\text{Kgm}^{-3}$	41.021	968
Dynamic Viscosity	Pa-s	$12.77 \times 10^{-6}$	0.145

---

## 2.4 CFD Modeling Approach

The refrigerant property input is based on NIST Refprop version 10.0. ANSYS Fluent 2020 R2 is used for analysis. DPM approach is useful for gas-liquid flows when dispersed phase occupies a low volume fraction (< 10%). In this case DPM approach is used. No particle to particle interaction and negligible effect of oil particles on the gas phase is assumed due to very low volume fraction (0.32%) of oil. The Reynolds number ( $Re > 397000$ ) is well over 4000 throughout the oil separator and piping which means the flow is turbulent. Steady state simulations are carried out considering uniform flow profile at gas inlet. SIMPLE pressure velocity coupling and second order upwind discretization is used. Demisters are modeled as porous medium using the viscous and inertial resistance coefficients as  $486707.9 \text{ m}^{-2}$  &  $439.4 \text{ m}^{-1}$  respectively.

### 2.4.1 Turbulence Model Selection

The k- $\omega$  models, which are more sensitive to near-wall effects are not selected as the primary focus is understanding the bulk flow and separation process than resolving the near-wall phenomena in great detail. Since the realizable k- $\epsilon$  model provides the best performance of all the k- $\epsilon$  models for flows involving separation, boundary layers under adverse pressure gradients, recirculation, it is selected.

### 2.4.2 Governing Equations for Continuous (Refrigerant Gas) Phase

$$\frac{\partial \rho}{\partial t} + \nabla \cdot (\rho \cdot \vec{v}) = S_m \quad (1)$$

' $S_m$ ' is the dispersed phase mass added to the continuous phase in mass conservation eq. (1)

$$\frac{\partial (\rho \vec{v})}{\partial t} + \nabla \cdot (\rho \vec{v} \vec{v}) = -\nabla p + \nabla \cdot (\bar{\tau}) + \rho \vec{g} + \vec{F} \quad (2)$$

Equation (2) is momentum conservation (Navier-Stokes) eq., where  $\vec{v}$  is velocity vector,  $p$  is the static pressure,  $\rho$  is the gas density,  $\vec{g}$  is the gravitational acceleration,  $\vec{F}$  is the external body force.

$$\bar{\tau} = \mu [ (\nabla \vec{v} + \nabla \vec{v}^T) - \frac{2}{3} \nabla \cdot \vec{v} I ] \quad (3)$$

In eq. (3),  $\bar{\tau}$  is the stress tensor,  $\mu$  is the molecular dynamic viscosity, and the unit tensor is  $I$ . The second term on the right hand side is the effect of volume dilation. The eq. for the kinetic energy of turbulence is given by

$$\frac{\partial}{\partial t} (\rho k) + \frac{\partial}{\partial x_j} (\rho k u_j) = \frac{\partial}{\partial x_j} \left[ \left( \mu + \frac{\mu_t}{\sigma_k} \right) \frac{\partial k}{\partial x_j} \right] + G_k + G_b - \rho \epsilon - Y_M + S_k \quad (4)$$

and

$$\frac{\partial}{\partial t} (\rho \varepsilon) + \frac{\partial}{\partial x_j} (\rho \varepsilon u_j) = \frac{\partial}{\partial x_j} \left[ \left( \mu + \frac{\mu_t}{\sigma_\varepsilon} \right) \frac{\partial \varepsilon}{\partial x_j} \right] + \rho C_1 S_\varepsilon - \rho C_2 \frac{\varepsilon^2}{K + \sqrt{\nu \varepsilon}} + C_{1\varepsilon} \frac{\varepsilon}{k} C_{3\varepsilon} G_b + S_\varepsilon \quad (5)$$

$$C_1 = \text{Max} \left[ 0.43, \frac{n}{n+5} \right] \quad (6)$$

$$n = S \frac{k}{\varepsilon} \quad (7)$$

$$S = \sqrt{2 S_{ij} S_{ij}} \quad (8)$$

In the eq. (4) and (5),  $G_k$  and  $G_b$  represent the generation of turbulence kinetic energies due to the mean velocity gradients and due to buoyancy respectively.  $Y_M$  is the contribution of the fluctuating dilatation in compressible turbulence to the overall dissipation rate.  $C_2$ ,  $C_{3\varepsilon}$  and  $C_{1\varepsilon}$  are the constants.  $\sigma_k$  and  $\sigma_\varepsilon$  are the turbulent Prandtl numbers for  $k$  and  $\varepsilon$ , respectively.  $S_k$  and  $S_\varepsilon$  are source terms.

### 2.4.3 Governing Equations for Discrete (Oil) Phase

The force balance eq. of one oil droplet is

$$\frac{d\vec{u}_p}{dt} = F_D (\vec{u} - \vec{u}_p) + \frac{\vec{g} (\rho_p - \rho)}{\rho_p} + \vec{F}_x \quad (9)$$

where the first item on the right-hand side is the drag force per unit particle mass. The coefficient  $F_D$  is

$$F_D = \frac{18\mu}{\rho_p d_p^2} \frac{C_D Re_p}{24} \quad (10)$$

Here,  $\vec{u}$  is the gas phase velocity,  $\vec{u}_p$  is the particle velocity,  $\rho_p$  is the density of the particle and  $d_p$  is particle diameter.  $C_D$  is the drag coefficient, and  $Re_p$  is relative Reynolds number are calculated as

$$Re_p = \frac{\rho d_p |\vec{u} - \vec{u}_p|}{\mu} \quad (11)$$

$$C_D = a_1 + \frac{a_2}{Re_p} + \frac{a_3}{Re_p^2} \quad (12)$$

Where  $a_1$ ,  $a_2$  and  $a_3$  are constants. The second item in eq. (9) is the gravity force per unit particle mass and the last term is the additional force, which is equal to the Saffman's lift force calculated as

$$\vec{F}_x = \frac{2Kv^{\frac{1}{2}}\rho d_{ij}}{\rho_p d_p (d_{lk}d_{kl})^{\frac{1}{4}}} (\vec{u} - \vec{u}_p) \quad (13)$$

where  $K = 2.594$ ,  $d_{ij}$  is the deformation tensor,  $\nu$  is the kinematic viscosity. Integrating eq. (9) over discrete time steps gives velocity & further integration gives the displacement i.e. droplet trajectory.

## 2.4.4 Coupling Between the Discrete and Continuous Phases

One-way coupling approach is implemented. The continuous phase always impacts the discrete phase. The momentum transfer between the continuous and discrete phase is computed & used in eq. (2) In eq.(14),  $\dot{m}_p$  is the mass flow rate of the oil droplets and  $\Delta t$  is the time step.

$$\vec{F} = \sum \left[ \frac{18\mu C_D Re_p}{24\rho_p d_p^2} (\vec{u}_p - \vec{u}) + \vec{F}_{other} \right] \dot{m}_p \Delta t \quad (14)$$

## 2.5 Boundary Conditions

Refer Fig. 3 for the boundary conditions for oil separators. The boundary condition type of oil separator's wall and baffles where flow is directly striking is set as 'Trap' as oil is most likely to separate in this region and all other internal surfaces are kept as 'Reflect', oil separator inlet & outlet is set as 'Escape' and oil outlet is set as 'Escape' while solving discrete phase.

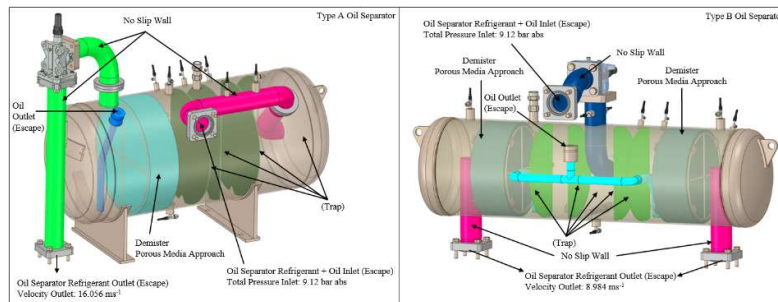


**Figure 3: Boundary conditions**

## 2.6 Details of Grid

Grid is created in Hypermesh and T-Grid using tetrahedral & prism element types. The maximum skewness is 0.88. Initially the problem is solved by using coarse grid and then by using refined grids, until results are close to asymptote as shown in Fig. 4. After 5.1 million grid size the variation in total pressure drop is < 0.03 %. Grid size of 5.6 million or higher is used for ensuring grid independency.

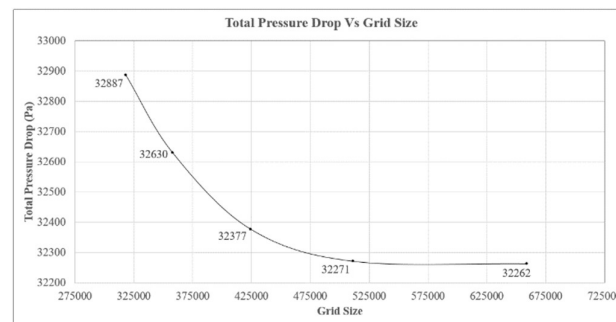


**Figure 4: Grid independent solution**

## 2.7 Post Processing Planes

Fig. 5 shows the post processing planes used in CFD result analysis.

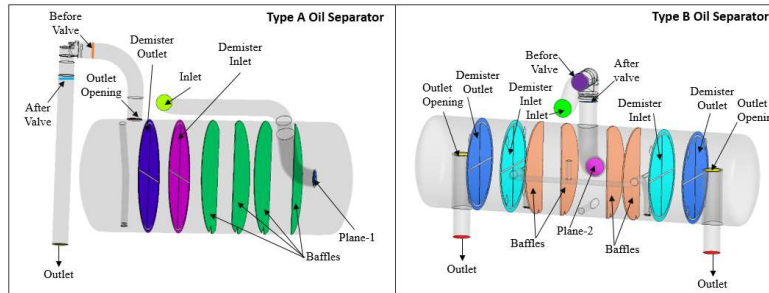


**Figure 5: Post processing planes**

## 3. Computational Result Analysis

### 3.1 Oil Separation Efficiency

Table 2 gives the oil separation efficiency with respect to oil droplet diameters. Oil separation efficiency increases with increase in droplet size. Both oil separators have 100 % oil separation efficiency at and above 25  $\mu\text{m}$  droplet diameter. Type B design is more efficient than Type A.

**Table 2: Oil separation efficiency**

Oil Droplet Diameter [ $\mu\text{m}$ ]	1	5	10	25	35	50	75	100	200	300	400	500
Type A Oil Separator	15	30	48	100	100	100	100	100	100	100	100	100
Type B Oil Separator	28	55	79	100	100	100	100	100	100	100	100	100

### 3.2 Velocity Distribution

Fig. 6 shows the velocity streamlines for oil separators. There are two outlet connections in Type B oil separator, therefore velocity is much lower at outlet to that of Type A oil separator.

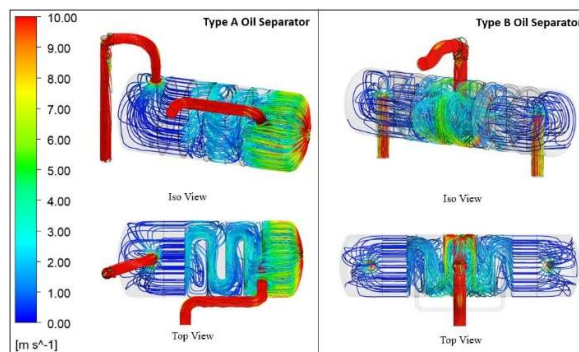


**Figure 6: Velocity Streamlines**

### 3.3 Pressure drop

Table 3 gives the breakup of pressure drop in oil separators. The optional discharge isolation valve is the highest contributor & demister pad is lowest contributor to the pressure drop in both designs. Shorter outlet piping and elbow elimination causes lower pressure drop in Type B oil separator. More baffles in Type A than Type B oil separator cause higher pressure drop from plane 1 to demister inlet.

**Table 3: Pressure drop in oil separators**

Pressure drop [Pa] :	Type A Design		Type B Design	
	Static	Total	Static	Total
Location				
Inlet to Plane-1	3423.48	1809.08	-	-
Inlet to Before Valve	-	-	463.91	298.20
Plane-1 or 2 to Demister Inlet	346.78	6934.50	-86.46	5366.51
Demister Inlet to Demister Outlet	162.80	176.55	145.02	153.14
Demister Outlet to Outlet Opening	10848.30	1556.35	2809.93	356.02
Outlet Opening to Before valve	-1538.23	2307.08	-	-
Before Valve to After Valve	23526.44	15699.34	19370.06	16031.45
After Valve to Outlet	-4219.08	3779.24	-	-
After Valve to Plane-2	-	-	-709.78	2455.13
Outlet Opening to Outlet	-	-	-354.76	407.28
Total Pressure Drop	32550.49	32262.14	21637.92	25067.72

### 3.4 Oil Droplet Trajectories

Fig. 7 shows the oil droplet path lines colored by residence time for various oil droplet sizes. Larger oil droplets have shorter trajectories and shorter residence time; hence larger droplets are easy to settle and separated. Splitting the flow reduces the required residence time in Type B oil separator.

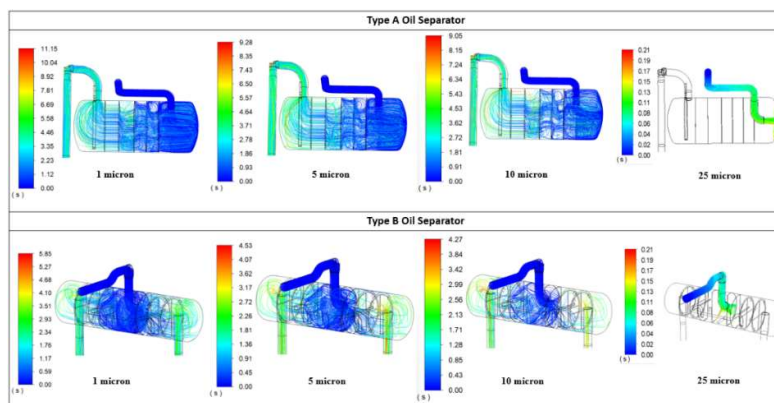


**Fig. 7: Oil Droplet Pathlines Colored by Residence Time**

#### 4. Experimental Set Up

Oil circulation rate (OCR) in liquid refrigerant is experimentally determined as per ASHRAE standard 41.4. [17] Fig. 8 shows the experimental test set up and schematic of oil content test. The liquid refrigerant is collected in sampling cylinders from the condenser outlet liquid line once the stable test conditions are achieved. The chillers are tested as per qualification plan.

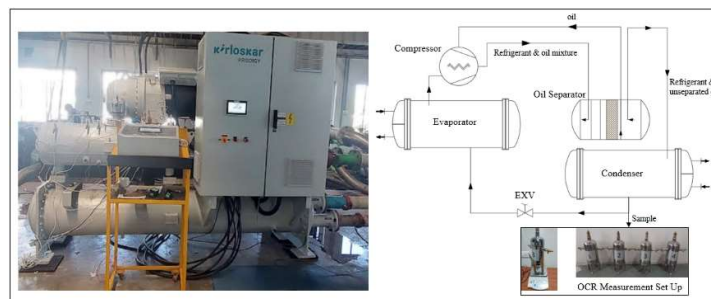


Fig. 8: Schematic of oil content test

Table 4 informs about the details of measuring instruments and uncertainty budget calculated as per NABL [18-19] standards.

**Table 4: Details of measuring instruments and uncertainty budget**

Measured Variable	Measuring Device	Unit	Range	Least Count	Accuracy	Expanded Uncertainty
Evap. water temperature	Temp. sensor	Deg C	(-)100 to 157	0.0001	± 0.1	± 0.05
Cond. water temperature	Temp. sensor	Deg C	(-)100 to 157	0.0001	± 0.1	± 0.06
Evaporator water flow	Flow meter	m <sup>3</sup> /hr	0 to 360	1	± 0.5 %	± 0.50
Condenser water flow	Flow meter	m <sup>3</sup> /hr	0 to 360	1	± 0.5 %	± 0.60
Voltage	Power meter	V	0 to 460	0.01	± 0.5 %	± 2.51
Current	Power meter	A	0 to 2500	0.01	± 0.5 %	± 0.91
Power	Power meter	kW	0 to 1150	0.0001	± 0.5 %	± 0.60
Water diff. pressure	Transducer	kg/cm <sup>2</sup>	0 to 5	0.01	± 0.015	± 0.01
Pressure Oil Sep. inlet	Pressure sensor	bar	0 to 9.3	0.001	1.20%	± 0.121
Pressure Oil Sep. outlet	Pressure sensor	bar	0 to 9.3	0.001	1.2 % FS	± 0.117
Weight	Machine	gram	0 to 6200	0.01	1.2 % FS	± 0.22

#### 5. Qualification Plan

Oil separators are designed for maximum flow rate and pressure drop. Separated oil is returned to compressor using the difference in pressure between oil (discharge) and suction. Oil separator must operate reliably at maximum flow rate conditions.

## 6. Test Results

Table 5 shows the pressure drop & OCR comparison for oil separators. The Type B oil separator has lower pressure drop than Type A oil separator at almost equivalent flow rate. The CFD computed pressure drop is in close agreement (< 5%) with the experimental pressure drop. Type B oil separator has lower oil circulation rates as compared to Type A oil separator. This is in-line with the CFD computed separation efficiency estimates.

**Table 5: Pressure drop & OCR comparison for oil separators**

Pressure Drop [Pa]	CFD Computed	Experimental	Mean OCR
Type A	32551 at 0.07649 [m <sup>3</sup> s <sup>-1</sup> ]	31500 at 0.07641 [m <sup>3</sup> s <sup>-1</sup> ]	0.49
Type B	21638 at 0.07649 [m <sup>3</sup> s <sup>-1</sup> ]	20500 at 0.07652 [m <sup>3</sup> s <sup>-1</sup> ]	0.48

Table 6 shows the comparison of chiller performance with Type A and Type B oil separators. Chiller with Type B oil separator is having 0.5 % more refrigeration capacity, 1.6 % better COP and 1.1 % lower power consumption than chiller with Type A oil separator.

**Table 6: Comparison of chiller performance with Type A and Type B oil separators**

Chiller with Oil Separator :	Type A	Type B	% Improvement
Capacity [kW]	499.29	501.73	0.5%
Power [kW]	93	92	1.1%
COP	5.37	5.45	1.6%

## 7. Conclusion

This study evaluates two oil separator designs for reducing the pressure drop, increasing the separation efficiency, at lower capital and operating cost for a screw chiller. CFD analysis provides a useful understanding of inside flow distribution which influence pressure drop and separation efficiency. The DPM is beneficial for computing oil droplet trajectories and comparing the oil separation efficiency. CFD simulation predicts the pressure drop closely. Velocity reduction improves the oil separator performance. Splitting the discharge flow is found useful to reduce the shell diameter, pressure drop and cost of oil separator. The coefficient of performance of chiller improves with the reduction of discharge pressure drop. The lower OCR rates at maximum flow conditions without oil level trips qualify both the oil separator designs. Model base design using CFD is useful tool for designing better oil separators.

## Acknowledgements

The authors are grateful to Kirloskar Chillers Pvt. Ltd., India for funding this research.

## Nomenclature

- $a_1, a_2, a_3$  - Constant [-]
- $C_2, C_{3\epsilon}, C_{1\epsilon}$  - Constants [-]
- $C_D$  - Drag coefficient [-]
- $d_p$  - Particle diameter [m]

---

$\Delta t$	- Time step [s]
$\varepsilon$	- Dissipation rate of turbulence kinetic energy [ $\text{m}^2\text{s}^{-3}$ ]
$\vec{F}$	- Force vector [N]
$\vec{F}_{other}$	- Other interaction forces per unit mass [N/kg]
$\vec{F}_x$	- Saffman's lift force [N]
$\vec{g}$	- Gravitational acceleration [ $\text{ms}^{-2}$ ]
$G_b$	- Turbulence kinetic energies due to buoyancy [ $\text{kgm}^{-1}\text{s}^{-2}$ ]
$G_k$	- Turbulence kinetic energies due to the mean velocity gradients [ $\text{kgm}^{-1}\text{s}^{-2}$ ]
$k$	- Turbulence kinetic energy [ $\text{m}^2\text{s}^{-2}$ ]
$K$	- Constant [-]
$\dot{m}_p$	- Mass flow rate of oil droplets [ $\text{kgs}^{-1}$ ]
$\mu$	- Molecular dynamic viscosity [Pas]
$p$	- Static pressure [Pa]
$Re$	- Reynold number [-]
$Re_p$	- Relative Reynolds number [-]
$\rho$	- Density [ $\text{kgm}^{-3}$ ]
$\rho_p$	- Density of the particle [ $\text{kgm}^{-3}$ ]
$\sigma_\varepsilon$	- Turbulent Prandtl numbers for $\varepsilon$ [-]
$\sigma_k$	- Turbulent Prandtl numbers for $k$ [-]
$S_\varepsilon$	- User-defined source term [ $\text{kgm}^{-1}\text{s}^{-3}$ ]
$S_k$	- User-defined source term [ $\text{kgm}^{-1}\text{s}^{-3}$ ]
$S_m$	- Mass added to the continuous phase from the dispersed second phase [ $\text{kgm}^{-3}\text{s}^{-1}$ ]
$\bar{\tau}$	- Stress tensor [Pa]
$\vec{u}$	- Fluid phase velocity [ $\text{ms}^{-1}$ ]
$\vec{u}_p$	- Particle velocity [ $\text{ms}^{-1}$ ]
$\nu$	- Kinematic viscosity [ $\text{m}^2\text{s}^{-1}$ ]
$\vec{v}$	- Velocity vector [ $\text{ms}^{-1}$ ]
$Y_M$	- Contribution of the fluctuating dilatation to the overall dissipation rate [ $\text{kgm}^{-1}\text{s}^{-2}$ ]

## References

- [1] Haider, S.A. et al., Oil Circulation Ratio Prediction in a Vapor Compression System Using a Discharge Side Oil Separator and Mass Flow Correction, *International Journal of Refrigeration*, Vol. 169 (2025), pp. 69-79, DOI: <https://doi.org/10.1016/j.ijrefrig.2024.09.02>
- [2] API 12J: 2008, *Specification for Oil and Gas Separators*, The American Petroleum Institute, Eighth edition, (2008)
- [3] Arnold K. and Stewart M., Two-Phase Oil and Gas Separation, in *Surface Production Operations: Design of Oil Handling Systems and Facilities*, Elsevier, (1999), Chapter 4, pp. 101-134, DOI: <https://doi.org/10.1016/B978-088415821-9/50005-1>
- [4] Jekel, T., et al., Gravity Separator Fundamentals and Design, *IAR 2001 Ammonia Refrigeration Convention & Exhibition*, Long Beach, CA, USA, (2001), pp. 1-23

- 
- [5] Wiencke, B., Fundamental Principles for Sizing and Design of Gravity Separators for Industrial Refrigeration, *International Journal of Refrigeration*, Vol. 34, Issue 8, (2011), pp. 2092-2108, DOI: <https://doi.org/10.1016/j.ijrefrig.2011.06.011>.
- [6] Bothamley M., Gas/Liquid Separators: Quantifying Separation Performance - Part 1, *Oil and Gas Facilities*, (2015), pp. 22-29, DOI: 10.2118/0813-0021-OGF
- [7] Bothamley M., Gas/Liquid Separators: Quantifying Separation Performance - Part 2, *Oil and Gas Facilities*, (2015), pp. 35-47, DOI: 10.2118/1013-0035-OGF
- [8] Xu, J., and Hrnjak, P. S., Formation, Distribution, and Movement of Oil Droplets in The Compressor, *International Journal of Refrigeration*, Vol. 93, (2018), pp. 184-194, DOI: 10.1016/j.ijrefrig.2018.06.020
- [9] Xu, J., and Hrnjak, P. S., Coalescing Oil Separator for Compressors, *International Journal of Refrigeration*, Vol. 106, (2019), pp. 41-53, DOI: <https://doi.org/10.1016/j.ijrefrig.2019.06.027>
- [10] Laleh A., et al., Design and CFD Studies of Multiphase Separators - A Review, *Canadian Society for Chemical Engineering*, Vol. 90, (2012), pp. 1547-1560
- [11] Laleh A., et al., Computational Fluid Dynamics-Based Study of an Oilfield Separator-Part I: A Realistic Simulation, Society of Petroleum Engineers, *Oil and gas facilities*, Vol. 90, (2012), pp. 57-68, DOI: 10.1002/cjce.20665
- [12] Gaffarkhah A, et al., Application of CFD for Designing Conventional Three Phase Oilfield Separator, *Egyptian Journal of Petroleum*, Vol. 26, Issue 2, (2017), pp. 313-420, DOI: 10.1016/j.ejpe.2016.06.003
- [13] Oliveira J. Jr., et al, Numerical Simulation of Demister Equipment for Application in Gravitational Separators, *Proceedings of COBEM 2009, 20<sup>th</sup> International Congress of Mechanical Engineering*, Brazil (2009), pp. 1-8.
- [14] Feng, J. M., et al., Investigation of the Oil-Gas Separation in a Horizontal Separator for Oil Injected Compressor Units, *Proceedings of the Institution of Mechanical Engineers, Part A Journal of Power and Energy*, Vol. 222, (2008), pp. 403-412, DOI: 10.1243/09576509JPE550
- [15] Wang Zhongyia, et al., The Analysis of Internal Flow Field in Oil-Gas Separator, *Procedia Engineering* 15, (2011), pp. 4337-4341, DOI: 10.1016/j.proeng.2011.08.814
- [16] Eastwick C. et al, Using CFD to Improve Aero-Engine Air/Oil Separator Design, *ASME PVP2002-1554*, (2002), pp. 215-220, DOI: 10.1115/PVP2002-1554
- [17] ASHRAE 41.4, Standard Method for Measurement of Proportion of Lubricant in Liquid Refrigerant, (1996), American Society of Heating, Refrigerating and Air-Conditioning Engineers
- [18] NABL-141, Guidelines for Estimation and Expression of Uncertainty in Measurement, Issue 02, (2000), National Accreditation Board for Testing and Calibration Laboratories India
- [19] NABL-174, Sample Calculations for Uncertainty of Measurement in Electrical Testing, Issue 02, (2004), National Accreditation Board for Testing and Calibration Laboratories India

Paper submitted: 22 January 2025  
Paper revised: 14 February 2025  
Paper accepted: 16 February 2025